# Electrically-driven ultrafast out-of-equilibrium light emission from hot electrons in suspended graphene/hBN heterostructures

OPEN ACCESS
IOP Publishing | IMMT
International Journal of Extreme Manufacturing
Int. J. Extrem. Manuf. **6** (2024) 015501 (11pp)
https://doi.org/10.1088/2631-7990/acfbc2

# Electrically-driven ultrafast out-of-equilibrium light emission from hot electrons in suspended graphene/hBN heterostructures

**Qiang Liu[1,2], Wei Xu[1,2], Xiaoxi Li[3,4], Tongyao Zhang[3,4], Chengbing Qin[4,5], Fang Luo[1,2,*], Zhihong Zhu[1,2], Shiqiao Qin[1,2,*], Mengjian Zhu[1,2,*] and Kostya S Novoselov[6,7]**

[1] College of Advanced Interdisciplinary Studies & Hunan Provincial Key Laboratory of Novel Nano-optoelectronic Information Materials and Devices, National University of Defense Technology, Changsha, Hunan 410073, People's Republic of China
[2] Nanhu Laser Laboratory, National University of Defense Technology, Changsha, Hunan 410073, People's Republic of China
[3] State Key Laboratory of Quantum Optics and Quantum Optics Devices, Institute of Opto-Electronics, Shanxi University, Taiyuan 030006, People's Republic of China
[4] Collaborative Innovation Center of Extreme Optics, Shanxi University, Taiyuan 030006, People's Republic of China
[5] State Key Laboratory of Quantum Optics and Quantum Optics Devices, Institute of Laser Spectroscopy, Shanxi University, Taiyuan 030006, People's Republic of China
[6] Institute for Functional Intelligent Materials, National University of Singapore, Singapore 117544, Singapore
[7] Department of Materials Science and Engineering, National University of Singapore, Singapore 117575, Singapore

E-mail: luofang2013@163.com, sqqin8@nudt.edu.cn and zhumengjian11@nudt.edu.cn

Received 26 June 2023, revised 27 July 2023
Accepted for publication 19 September 2023
Published 3 October 2023

**Abstract**

Nanoscale light sources with high speed of electrical modulation and low energy consumption are key components for nanophotonics and optoelectronics. The record-high carrier mobility and ultrafast carrier dynamics of graphene make it promising as an atomically thin light emitter, which can be further integrated into arbitrary platforms by van der Waals forces. However, due to the zero bandgap, graphene is difficult to emit light through the interband recombination of carriers like conventional semiconductors. Here, we demonstrate ultrafast thermal light emitters based on suspended graphene/hexagonal boron nitride (Gr/hBN) heterostructures. Electrons in biased graphene are significantly heated up to 2800 K at modest electric fields, emitting bright photons from the near-infrared to the visible spectral range. By eliminating the heat dissipation channel of the substrate, the radiation efficiency of the suspended Gr/hBN device is about two orders of magnitude greater than that of graphene devices supported on $SiO_2$ or hBN. We further demonstrate that hot electrons and low-energy acoustic phonons in graphene are weakly coupled to each other and are not in full thermal equilibrium. Direct cooling of high-temperature hot electrons to low-temperature acoustic phonons is enabled by the

* Authors to whom any correspondence should be addressed.


2631-7990/24/015501+11$33.00

significant near-field heat transfer at the highly localized Gr/hBN interface, resulting in ultrafast thermal emission with up to 1 GHz bandwidth under electrical excitation. It is found that suspending the Gr/hBN heterostructures on the $SiO_2$ trenches significantly modifies the light emission due to the formation of the optical cavity and showed a ∼440% enhancement in intensity at the peak wavelength of 940 nm compared to the black-body thermal radiation. The demonstration of electrically driven ultrafast light emission from suspended Gr/hBN heterostructures sheds the light on applications of graphene heterostructures in photonic integrated circuits, such as broadband light sources and ultrafast thermo-optic phase modulators.

Supplementary material for this article is available online

Keywords: suspended graphene, ultrafast light emitter, van der Waals heterostructures, thermal radiation, electron–phonon interaction

## 1. Introduction

With the development of silicon-based transistors approaching the physical limit of sub-5 nm nodes, photonic integrated circuits have been extensively studied over the past few decades, and are considered to be one of most promising routes for information technology in the post-Moore era [1–3]. Benefiting from the superior electronic and optical properties, graphene has shown great potential in nanophotonic and optoelectronic applications [4–6]. For instance, ultrafast and broadband photodetectors up to 500 GHz are achieved by integrating graphene with metamaterials [7–13]. It is also able to realize ultrafast optical modulators with a speed of 60 GHz and an efficiency of 2.25 $fJ{\cdot}bit^{-1}$ by integrating double-layer graphene devices onto silicon photonics platforms [14–21]. Many efforts have demonstrated the ultrafast photoluminescence from graphene excited by ultrashort femtosecond laser pulses, which can be understood by thermal emission or hot plasmon emission from photo-excited hot carriers in graphene [22–27]. However, due to the zero bandgap property, electrons rapidly relax by electron–electron and electron–phonon scattering, prohibiting the light emission through interband electron–hole recombination. Therefore, electrically-driven light emission from intrinsic graphene remains a substantial challenge.

Recently, light emission has been successfully reported from electrically biased graphene devices due to the gray-body thermal emission. Since most of the energy is dissipated through the substrates, $SiO_2$-supported graphene devices show limited temperatures of ∼1500 K, emit infrared light, and have very low radiation efficiencies of $\sim10^{-6}$ [28–32]. The temperature and the radiation efficiency can be greatly enhanced by suspending graphene on trenches, reaching ∼2800 K and $\sim10^{-3}$ for monolayer graphene devices, respectively [33]. As a result, suspended graphene devices can emit significant visible light under vacuum. However, conventional suspend devices are very fragile and graphene membranes often collapse and rupture during fabrication and measurement [34, 35]. As a two-dimensional insulator, hexagonal boron nitride (hBN) provides an excellent encapsulation of graphene, enabling electron temperature of graphene up to ∼2100 K and producing wide spectral range emission from infrared to visible [36–41]. Under pulsed voltage excitation, hBN encapsulated graphene devices demonstrate high-speed electrical modulation up to 3 GHz. The observation of fast modulation was attributed to the efficient cooling process of hot carriers in biased graphene via the near-field heat dissipation at the graphene/hBN (Gr/hBN) hybrid interface [36]. However, the radiation efficiency of hBN encapsulated graphene emitters is still limited to $\sim3\times10^{-6}$, which is mainly due to the significant heat transfer from graphene to substrate underneath [32]. So far, it remains a great challenge for graphene light emitters to simultaneously exhibit high temperature, high thermal radiation efficiency and fast modulation rate. Moreover, reducing the heat transport channels in suspended devices is thought to limit the rate of cooling for fast modulation [33, 36]. In addition, the modulation speed of suspended graphene heterostructure thermal emitters under electrical excitation has not yet been studied.

In this work, we develop a van der Waals (vdW) integration strategy for the controlled fabrication of suspended graphene devices by one-step direct transfer of Gr/hBN heterostructures onto metallic electrode trenches on silicon platforms. The strong adhesion between hBN and graphene greatly enhances the mechanical strength of the suspended membranes, effectively prevents graphene from collapsing, cracking, and curling defects, and does not require a complex critical point drying process. Based on high-quality suspended heterostructures, we demonstrate ultrafast thermal light emitters driven by high-frequency ac electrical inputs. Under Joule heating by bias electric fields, the electronic temperature of graphene reaches up to 2800 K, emitting bright photons with a broadband spectrum from the visible to the near-infrared range. The resulting hBN/$SiO_2$ dielectric optical cavity strongly modifies the emission spectrum, and the emission intensity at 940 nm is increased by ∼440% compared to the gray-body radiation of monolayer graphene. In-situ measurements of electron temperature and phonon temperature show that the temperature of electrons at high bias voltages is more than three times higher than that of low-energy acoustic phonons due to the weak coupling and non-equilibrium between the hot electrons and the acoustic phonons of graphene. Our devices show

ultrafast emission response when excited by radiofrequency electrical signals. The full width at half-maximum (FWHM) and electrons heating and cooling times of the response are determined as ∼1.5 ns and ∼0.9 ns, respectively, the latter indicates an operation bandwidth above 1 GHz. The analysis of the hot electron cooling pathway shows that the hot electrons are in equilibrium with high-energy optical phonons, and are strongly coupled to the hybrid plasmon-phonon polariton at the Gr/hBN interface, but not in a full thermal equilibrium with the low-energy acoustic phonons. Thus, the high-speed response of the thermal emission in suspended Gr/hBN is possibly due to the ultrafast cooling of hot electrons to acoustic phonons, which is sufficient to modulate the radiation intensity.

## 2. Results and discussion

### *2.1. Fabrication and characterizations of the suspended devices*

Metal electrodes (270 nm thick Au) were deposited on 285 nm-$SiO_2$/Si substrate by UV lithography and electron-beam evaporation techniques. Graphene and hBN flakes were mechanically exfoliated and assembled into Gr/hBN vdW heterostructures by a polymer assisted dry-transfer method [42]. Then, the stacks were transferred onto the pre-fabricated electrode trenches to form suspended Gr/hBN heterostructure devices, as shown in figure 1(a). The final step removes the polymer layer by chloroform dissolution or high vacuum annealing without using critical point dryer or hot acetone. Supporting information (SI) section S1 and figure S1 describe more details of the device fabrication process. Compared with the conventional methods of preparing suspended graphene devices, our strategy exhibits at least three advantages: (i) during the whole device fabrication processes, the graphene is subjected to hBN thin flake without contact with any solution, thereby well protected against collapse and breakage caused by surface tension changes; (ii) the excellent mechanical properties of hBN provide effective adhesion for suspended graphene via interfacial vdW interaction, significantly enhancing the mechanical strength of suspended Gr/hBN heterostructure devices [43]; (iii) hBN exhibits an atomically flat surface without dangling bonds, which reduces the source of carrier scattering in graphene. Furthermore, hBN is an insulator which has a band gap of ∼5.8 eV, so it does not affect the black-body radiation from biased graphene devices in the infrared to the visible spectrum range [44]. The number of layers of graphene and the thickness of hBN were determined by Raman spectroscopy and atomic force microscopy (AFM) measurements, respectively, as shown in figure S2. Figures 1(b) and (c) are optical microscopic image and scanning electron microscopy (SEM) image of a typical suspended Gr/hBN heterostructure device, respectively. By tilting the sample in SEM chamber, the suspended structure can be clearly resolved. No obvious defects such as collapse, breaks and wrinkles were observed in microscopy characterizations. More than ten devices were fabricated in this work and the suspension success rate was found to be ∼80% for a trench depth of 270 nm, as shown in table S1. Additional devices with different number of layers of graphene and aspect ratios are shown in figure S3. To improve contact transparency and remove chemical residues as much as possible, the suspended devices were annealed at 400 °C for 3 h under a high vacuum of $\sim 10^{-4}$ mbar. Two-terminal electrical measurements show smooth $I - V_g$ and ohmic linear $I - V_b$ characteristics of graphene ($I$ is the current, $V_g$ and $V_b$ are the back gate voltage and the bias voltage, respectively). The determined electron mobility and density ($V_g = 0$ V) at room temperature are $\sim 10^4$ cm$^2$·V$^{-1}$·s$^{-1}$ and $\sim 1.6 \times 10^{11}$ cm$^{-2}$, respectively, comparable to graphene devices encapsulated by commercial hBN crystals. The corresponding conduction band Fermi energy of graphene is ∼0.05 eV.

### *2.2. Temperatures of acoustic phonons and electrons in graphene*

The electric current flowing through the suspended graphene leads to Joule heating in the device, which effectively heats up the electrons and phonons of graphene. Under high electric fields up to 1.68 V·$\mu$m$^{-1}$ ($F = V_b/W$), the current density ($J = I/(W \cdot L)$, $W$ and $L$ are the width and length of graphene device) reaches $\sim 10^8$ A cm$^{-2}$ at $\sim 10^{-4}$ mbar vacuum. The electrons in graphene obtain very high kinetic energy after being accelerated by a strong electric field. Graphene exhibits ultra-low electronic heat capacity, resulting in a large temperature increase upon a small electric excitation. The noise thermometry measurement results show that the heat capacities of graphene is as low as $2 \times 10^{-9}$ J·m$^{-2}$·K$^{-1}$, recently even reaches a record-low value of $1.2 \times 10^{-11}$ J·m$^{-2}$·K$^{-1}$ [45, 46]. The excited electrons are rapidly equilibrated over several 100 fs timescales by electron–electron scattering to produce a hot electron distribution, and these specific electrons are called hot electrons. The hot electrons distribution is then relaxed on a few ps timescale by electron–phonon scattering. During this period, hot electrons at a given temperature ($T_e$), are not in full thermal equilibrium with the phonons [47]. Since heat dissipation mainly occurs through the transport of acoustic phonons, here we define the temperature of phonons ($T_{ap}$) as the lattice temperature ($T_L$).

Based on the frequency shift of graphene Raman G mode phonons, we can measure the temperature of the acoustic phonons of graphene by Raman spectroscopy [48]. Due to anharmonic phonon coupling, the G mode of graphene and the $E_{2g}$ mode of hBN undergo down-shift to lower wavenumbers as the lattice temperature increases. Temperature coefficient was defined as the ratio between Raman shift and temperature $\gamma = \Delta f/\Delta T$, calibrated by measuring the Raman peak positions as a function of increasing temperature. The devices were placed on a hot plate with adjustable temperature up to 1100 K in a $\sim 10^{-4}$ vacuum chamber. Under this steady condition, the heating is uniform in graphene and the temperatures of electrons and phonons are equal. All the positions of graphene G, 2D, and hBN $E_{2g}$ peaks show monotonic downshifts with increasing temperatures, as shown in section S2 and figure S4.

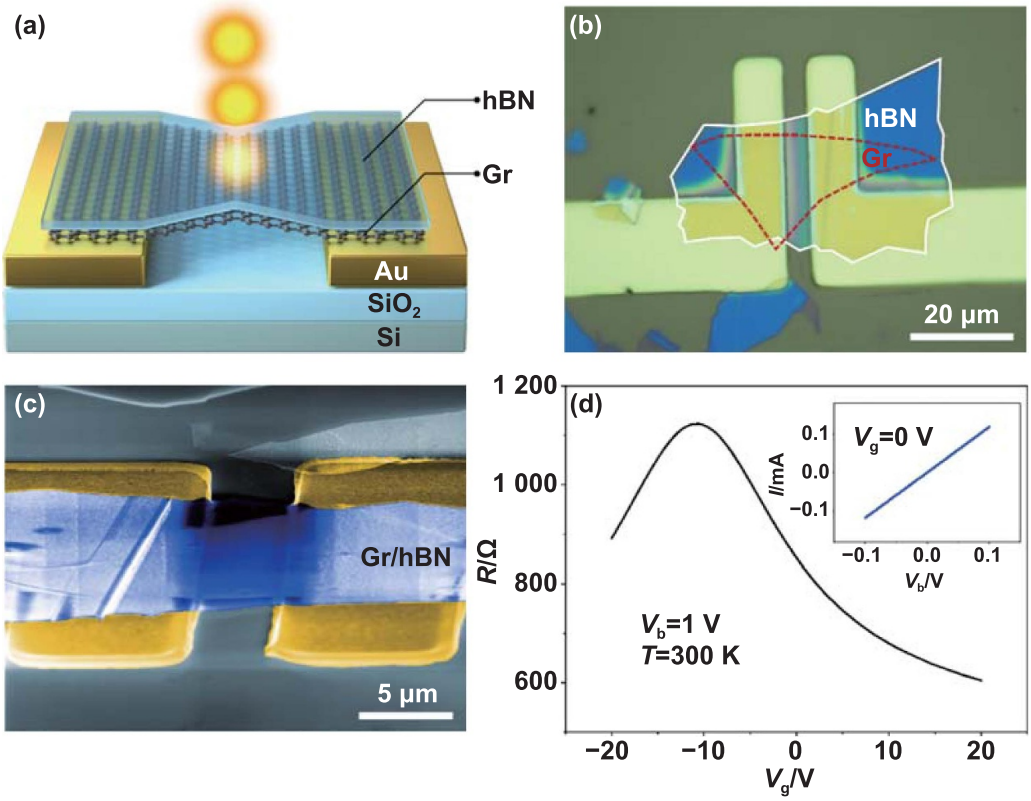


**Figure 1.** Suspended Gr/hBN heterostructure light emitter. (a) Schematic of the ultrafast graphene light emitter. The device structure includes a monolayer graphene and a thin hBN capping layer. (b) Optical microscopy image of a typical suspended device. (c) SEM image of the suspended device. The width and length of the suspended graphene region were measured to be ∼4.8 and ∼17.6 $\mu$m, respectively. (d) Field-effect curve ($I - V_g$) of the suspended device and the corresponding $I - V_b$ characteristics (inset).

Figure 2(b) summarizes the peak positions of the three main Raman modes as a function of environment temperature. For high temperature up to 1100 K, the downshift of the G, 2D and $E_{2g}$ modes are approximated linear functions of the heterostructure equilibrium temperatures, and the Raman temperature coefficient $\gamma$ can be determined. We then switched to Joule heating experiments, applying various $V_b$ to the suspended devices. As shown in figure S5, by combining Raman spectroscopy with spontaneous optical emission measurements, we were able to obtain independent information on the temperature of phonons and electrons in suspended graphene with current flow. Figures 2(c)–(e) show the evolution of these Raman modes at the center of the suspended Gr/hBN heterostructure at electric fields up to $1.68\,\mathrm{V}\cdot\mu\mathrm{m}^{-1}$. From the Raman map of the entire suspended region, the spatial distribution of lattice temperature of graphene can be further deduced by extracting the Raman peak evolution as a function of electric field. Here, we focus on the temperatures of acoustic phonons originating from the downshifts of the G mode, since extracting phonon population from the 2D mode is generally challenging [3]. As shown in figure 2(f), the outline of suspended graphene region can be clearly resolved by recording the local lattice temperature. The corresponding temperatures of acoustic phonons range from 292 to 960 K under an electric field of $1.68\,\mathrm{V}\cdot\mu\mathrm{m}^{-1}$. In general, the middle of graphene is hot, while the graphene near the contacts and the edges are cold. Along the $x$-direction, the temperature distribution is symmetrical: the temperature is highest in the center and gradually decreases towards the contacts. This can be explained by the fact that most of the heat is dissipated through the interface between the graphene and the metal electrodes by surface polar phonon scattering. Meanwhile, the temperature in graphene hardly changes along the $y$ direction, except for two suspending edges. By solving the steady-state heat diffusion equation: $-\nabla\cdot(\kappa\nabla T) = \dot{q}$, we calculated the graphene lattice temperature, where $\kappa$ is the thermal conductivity of graphene, $T$ is the graphene lattice temperature, and $\dot{q}$ is the input electrical power. More details of the numerical simulation can be found in section S3. Figure 2(i) is the simulated temperature distribution of the suspended device, which is quantitatively consistence with the experimental data, as shown in figures 2(g) and (h). The deviation between the experimental data (figure 2(f)) and the simulation (figure 2(i)) is mainly due to the non-uniform strain and defect distribution in suspended graphene/hBN devices. Due to its own mass, the strain distribution in graphene heterostructure is non-uniform, the strain in the center is maximum, while the strain on the edges is minimal. In addition to strain, random defects also can affect the accuracy of lattice temperature measurement by Raman spectroscopy.

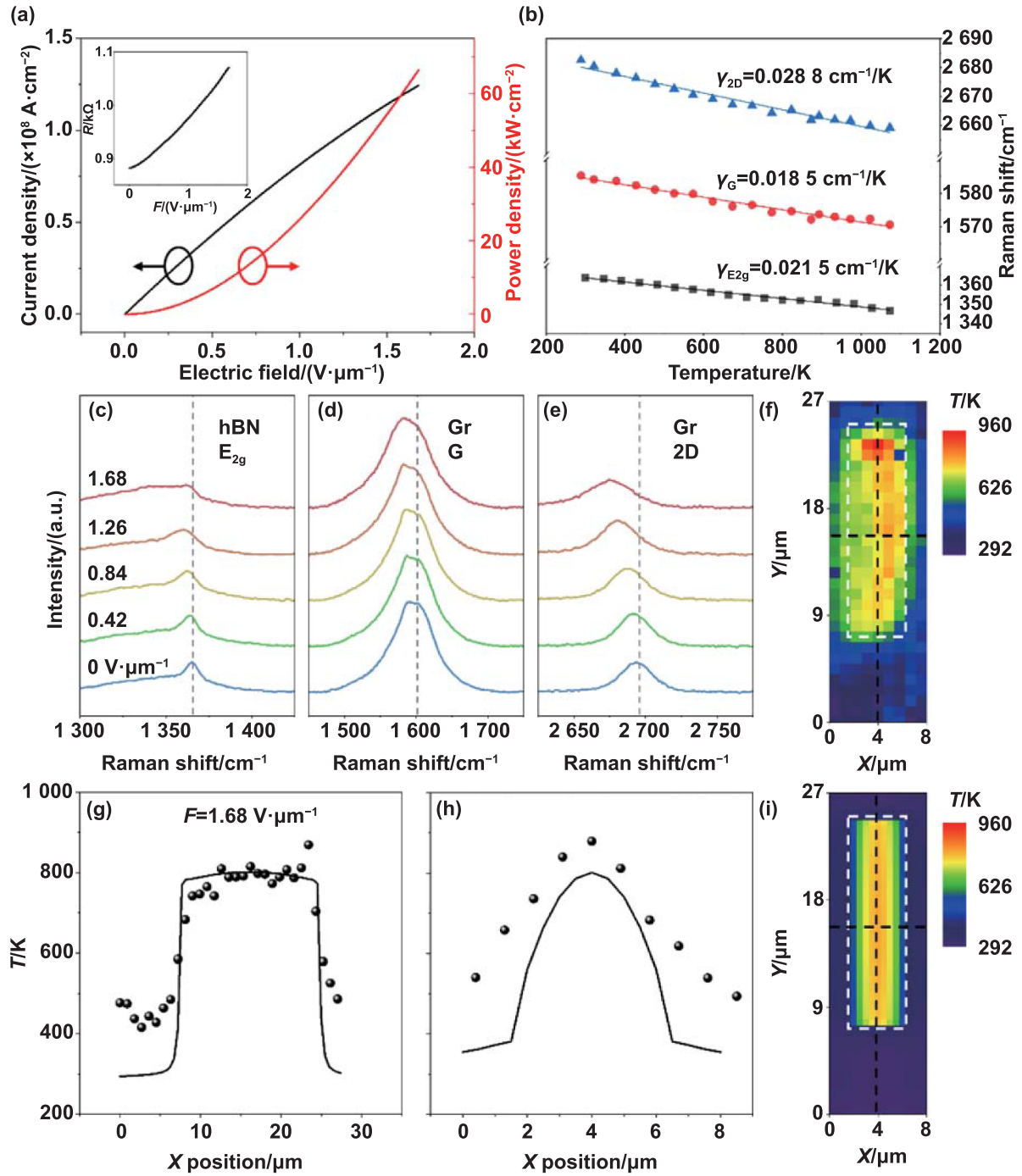


**Figure 2.** Probing the temperature of acoustic phonons of graphene by Raman spectroscopy. (a) Current density ($J$) and power density ($P$) as a function of applied bias electric field ($F$). The inset is the measured resistance ($R$) as a function of $F$. (b) The positions of Raman bands of graphene G and 2D and hBN $E_{2g}$ peaks as a function of temperature. The dashed lines are linear fits. (c)–(e) Raman spectra of suspended Gr/hBN heterostructure under various $F$. The dashed lines mark the Raman peak positions at $F = 0$. (f) Spatial distribution of graphene lattice temperature determined from Raman map of G peaks. (g) and (h) Vertical and longitudinal temperature profile of graphene. Solid dots are extracted experimental data, and curves are from simulation. (i) Simulated temperature distribution of graphene lattice. In (f) and (i), the white dashed shapes mark the suspended graphene regions, and the black dashed lines indicate the center position along $x$ and $y$ directions, respectively.

Light emission has been demonstrated from $Si/SiO_2$ supported, suspended and hBN encapsulated graphene devices. So far, no experimental investigation on suspended Gr/hBN heterostructure emitters has been reported. Figure 3(a) shows the light emission spectra of our suspended heterostructure device under different electric fields. Photon intensity rapidly increases with increasing the electric fields (or electric power). By increasing $F$ from 1.16 to 1.72 $V \cdot \mu m^{-1}$, the photon intensity is significantly enhanced by more than three orders of magnitude (∼2000-fold). As $F$ increases, the

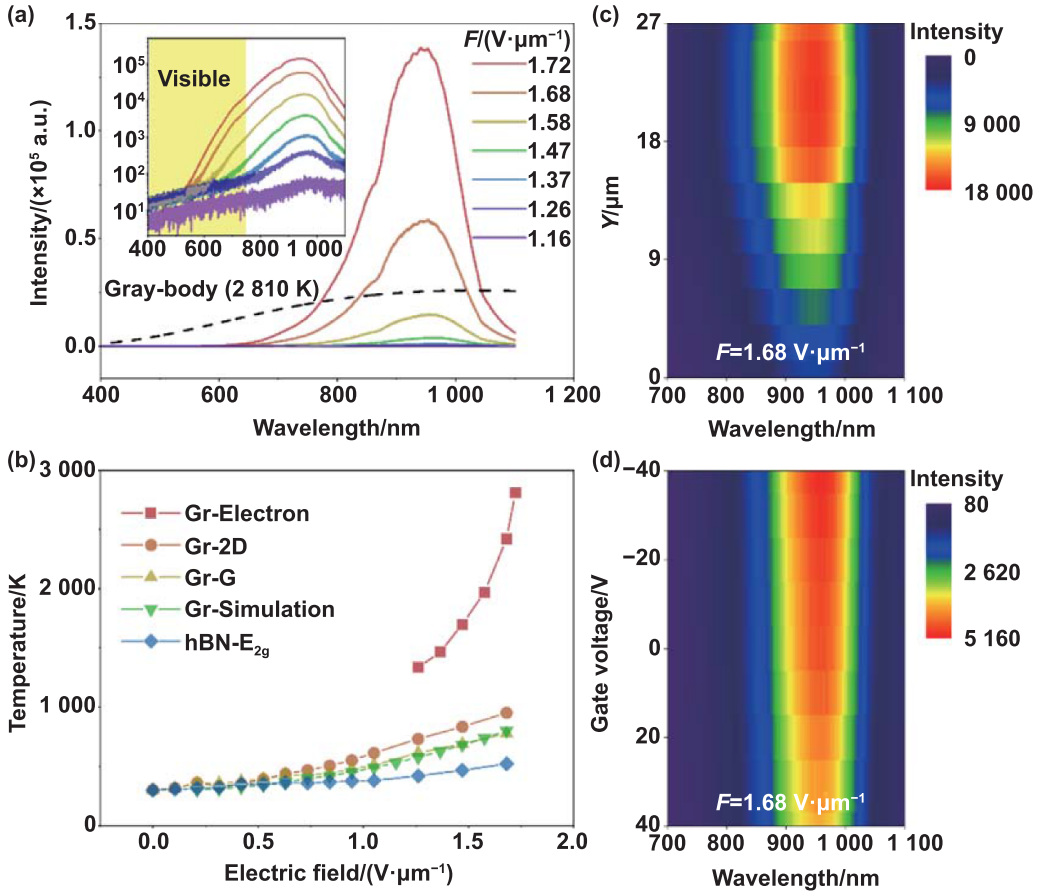


**Figure 3.** Light emission and electronic temperature of graphene. (a) Emission spectra of suspended Gr/hBN light emitter under various electric fields. Black dashed curve is the calculated gray-body radiation of monolayer graphene at 2810 K without optical cavity enhancement. The inset shows log scale data on the $y$ axis. The yellow shape in the inset marks the visible spectral range. (b) Determined various temperatures of the electrons and phonons in suspended Gr/hBN heterostructures. The values of $T_e$ were extracted from the fitting of the emission spectra and the values of $T_{ap}$ of graphene and hBN are estimated from the Raman shifts. (c) Light emission spectra at the middle position of suspended graphene along the vertical $y$ direction. (d) Gate dependence of the emission spectra at the center position of suspended graphene.

intensity enhancement is associated with the blue shifts of the center wavelength of the emission spectra, as shown in figure S6. For instance, the center peak wavelengths are 980 nm and 940 nm for 1.16 and $1.72\,\mathrm{V}\cdot\mu\mathrm{m}^{-1}$, respectively. We note that for $F > 1.47\,\mathrm{V}\cdot\mu\mathrm{m}^{-1}$, the emission spectra contain significant components of visible photons (400–760 nm). This is consistence with the optical microscopy image of the suspended device, which shines visible light under a modest electric field, as shown in figure S7. The strong near-infrared emission peaks were further attributed to the photonic cavity formed by the dielectric layers in the suspended device, including hBN, vacuum, and $SiO_2$. As a result, the local optical density of states is modified, leading to a tailored light emission spectrum. By using the above parameters, we were able to fit the experimental spectra with a simple model, as shown in section S4 and figure S8. We determined the electron temperature $T_e$ from the spectral fitting of spectra based on the optical cavity modulation. For $F = 1.72\,\mathrm{V}\cdot\mu\mathrm{m}^{-1}$, a maximum $T_e \sim 2810\,\mathrm{K}$ was extracted. According to Wien's displacement law, the peak position at the center wavelength $\lambda_{max}$ is given by: $\lambda_{max} = b/T$, where $T$ is the absolute temperature in Kelvins, $b$ is the Wien's displacement constant, equal to 2897.8 K·$\mu$m. Therefore, it can be clearly deduced that higher equivalent blackbody temperatures mean shorter radiation center wavelengths, which implies that the spectrum undergoes a blue shift as the temperature increases. We plotted the peak position of thermal emission as a function of the electron temperature of graphene, as show in figure S9. It is also found that the radiation enhancement can reach ~440% at the 940 nm center wavelength compared to the gray-body radiation from graphene. We consider the thermal radiation efficiency ($\eta$) at all the wavelength based on the Stefan–Boltzmann law, $J = \epsilon\sigma T^4$, where $\epsilon = 2.3\%$ is the emissivity of monolayer graphene, $\sigma = 5.67 \times 10^{-8}\,\mathrm{W}\cdot\mathrm{m}^{-2}\cdot\mathrm{K}^{-4}$ is the Stefan's constant. Under a steady state, we derived $\eta \sim 1.3 \times 10^{-4}$, which is two orders of magnitude higher than the radiation efficiency of the graphene devices supported on $SiO_2$ or encapsulated by hBN. Wavelength-dependent enhancements of radiation efficiency can be further engineered and enhanced by integrating the graphene emitters with plasmonic structures, optical cavities, photonic crystals, and so on.

Figure 3(b) shows the derived $T_e$ as a function of $F$, and the above estimated acoustic photon temperatures of graphene and hBN. The lattice temperature of hBN is slightly lower than that of graphene, which is mainly caused by the vertical interfacial thermal resistance [36]. Under modest electric fields ($F > 1.26\,\mathrm{V}\cdot\mu\mathrm{m}^{-1}$), the $T_{ap}$ of both graphene and hBN is significantly lower than the electronic temperature of graphene. For example, at $F = 1.68\,\mathrm{V}\cdot\mu\mathrm{m}^{-1}$, $T_e \sim 2420\,\mathrm{K}$ is three times of $T_{ap} \sim 800$ K in graphene. Such observation suggests that although the secondary phonons of graphene are substantially heated up and can reach temperature up to 800 K, the hot electrons however are not in full equilibrium with the lower-energy acoustic phonons of graphene. The behavior of hot electrons in electrically biased graphene has been reported in both substrate-supported graphene and suspended graphene light emitters [29, 33]. For $SiO_2$ or hBN supported graphene devices, $T_e$ and $T_{ap}$ reach maximum values of ∼2000 K and ∼1000 K, respectively [30, 36, 38, 40]. In our case, $T_e$ is much higher and can reach ∼2800 K at high bias, but the values of $T_{ap}$ of graphene are significantly lower ∼800 K. We know that in graphene devices supported by substrates with high electric fields, optical phonons are in equilibrium with electrons at temperatures up to ∼2000 K, but optical phonons and acoustic phonons are not in full equilibrium with each other because optical phonons decay at a much slower rate to acoustic phonons than that of optical phonons to electron–hole pairs [29, 30]. Because the heat cannot be dissipated to the substrate in our suspended Gr/hBN heterostructure devices, the temperatures of electrons and optical phonons are much higher than those in substrate-supported graphene devices. Thus, the electrons in graphene are highly decoupled from its lattice phonons, allowing for relatively cold graphene lattices and electrodes, while the electron system is very hot. This unique thermal decoupling mechanism can generate a highly efficient out-of-equilibrium light emission from the suspended Gr/hBN heterostructures before the device fails at high temperature. Such special temperature coupling opens up a wide design space for thermal emission control, which is challenging or impossible for heated conventional metal or semiconductor nanomaterials. As shown in a previous study, suspended Gr/hBN light emitter can be further integrated with Si-based photonic crystal, so that emission spectrum can be selectively tailored from a broad band gray body radiation to a desired narrow band thermal emission [40]. Furthermore, the light emission intensity along the suspended graphene region is fairly uniform and can be effectively modified by applying an external gate voltage, as shown in figures 3(c) and (d). The latter is attributed to the gate-tunable carrier concentration and current density.

### *2.3. Ultrafast light emission from suspended Gr/hBN heterostructures*

Benefiting from the small volume and ultra-low heat capacity of graphene, electrically-driven ultrafast light emitter can be realized by controlling the heating and cooling process of the electrons of graphene. Therefore, we measured the response speed of our suspended devices under an ac bias voltage $V_{ac}$. The setup of measurement is shown in SI section S5 and figure S10, where the emission of Gr/hBN was recorded by a silicon-based single-photon avalanche diode (SPAD). As shown in figure 4(a), graphene emitter can be visualized by recording the thermal emission intensity under $V_{ac} = 5\,\mathrm{V}$. After calibration, a series of mixed dc and ac voltages ($V_{dc} = 2\,\mathrm{V}$, $V_{ac} = 3.8\,\mathrm{V}$) were applied to the graphene emitter. Time-correlated single-photon counting system was applied to record the time-resolved spectra. Figure 4(b) shows typical ultrafast light emission excited by ac electric pulses with a fixed repetition rate of 10 MHz ($t = 100\,\mathrm{ns}$), but different duration $\Delta t_{ac} = 1.7$ and 5.0 ns, respectively. The time-resolve spectrum demonstrates that the extracted FWHM of response times are 1.5 and 2.6 ns, which are shorter than the excitation duration and are dominated by a relatively slow response from the electrical signal generator. As shown in figure 4(c), for all $\Delta t_{ac}$ from 45 ns to 1.7 ns, the linear slope between the photon emission width $\Delta t_{ph}$ and the electric pulse duration $\Delta t_{ac}$ is found to be close to unity, which also indicates the intrinsic response time of the suspended heterostructure light emission faster than experimentally obtained. The photon emission time trace in figure 4(d) shows excellent switching modulation and near-perfect contrast when the device is driven by a continuous electrical signal but varies at a repetition rate of 10–40 MHz.

We further extracted the rise time (10%–90% intensity) and the fall time (90%–10% intensity) from the emission spectrum at the 1.7 ns excitation. Both of them were determined as ∼0.9 ns, as shown in figure S11. This observation suggests that the heating and cooling processes in suspended heterostructure emitter are below 1 ns, mainly limited by the measurement setup. Notably, the heating and cooling response are symmetric and the time-resolved spectrum can be fitted by a single peak Gaussian formula, which is fundamentally different with previous reports on substrate-supported graphene thermal emitters. For graphene emitters on $SiO_2$ or hBN substrates, the cooling is rather slow compared to the rapid heating process and usually consists of two decay components [32, 36]. The first fall process is fast, corresponding to the electron cooling due to electron–phonon scattering, while the second one is due to much slower vertical heat dissipation through the underlying substrates. In our case, the lack of substrate eliminates the heat dissipating substrate. At the same time, due to Umklapp phonon–phonon scattering, the thermal conductivity of graphene at high temperature is greatly reduced, and the in-plane heat dissipation through the contacts is also effectively suppressed [49]. Thus, the reduction of energy dissipation channels effectively creates hot spots in the middle of graphene. The temperature response time of the heating process is on the order of 100 ps, consistent with previous reports [32, 36]. On the contrary, the lack of dissipation channels was considered to slow down the cooling process of electrons, limiting the modulation speed of suspended graphene thermal emitters [33]. Here, we demonstrate for the first time that electrons can cool down as fast as they heat up in suspended Gr/hBN heterostructure thermal emitters. Driven by a continuous 0.6 GHz electrical signal, the effective cooling of hot electrons in graphene appears as switching modulation

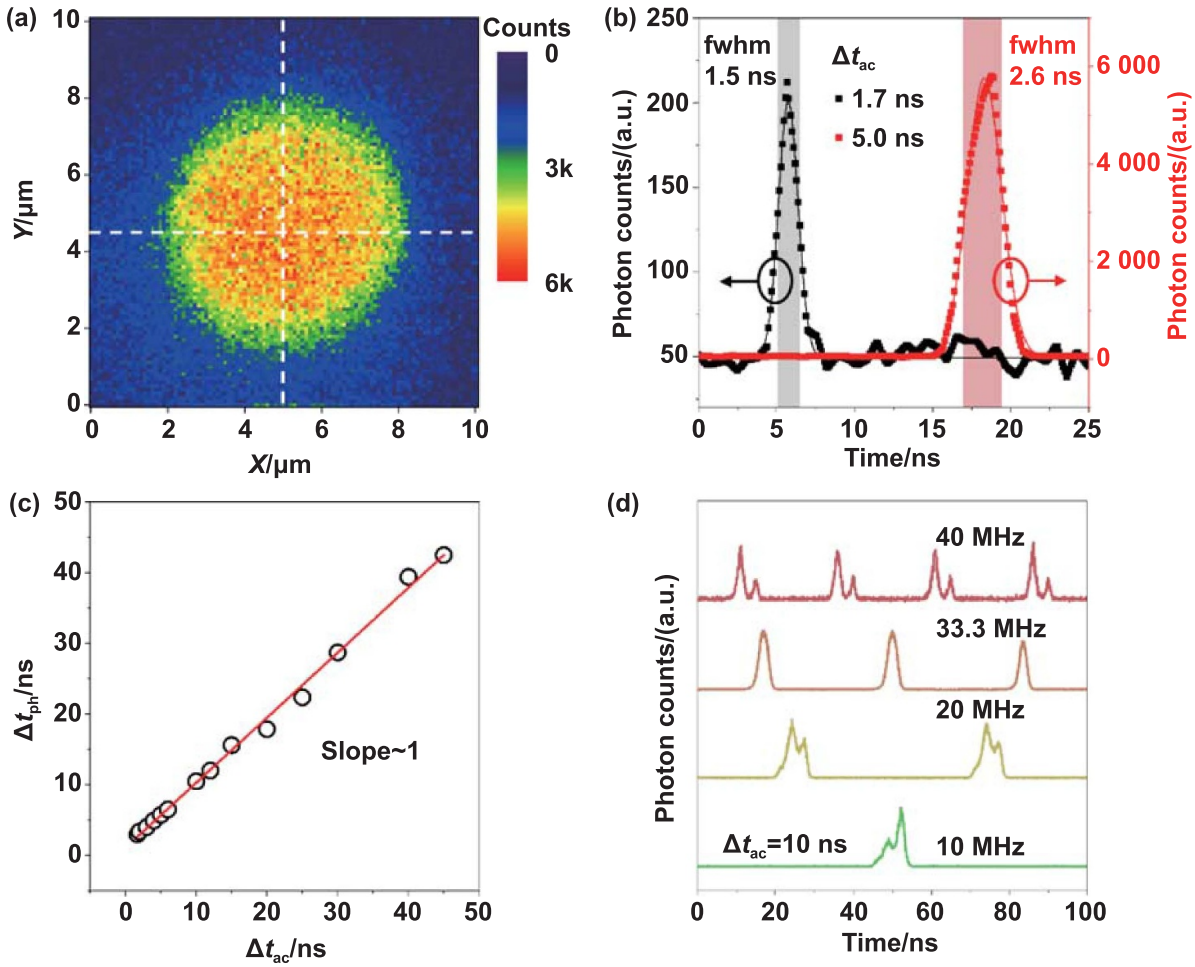


**Figure 4.** Ultrafast light emission from suspended Gr/hBN heterostructures. (a) Mapping light emission via a SPAD to locate the center of the suspended emitter. The device is biased by an ac voltage $V_{ac} = 5\,V$. The dashed cross marks the center of the suspended graphene. (b) Typical ultrafast thermal radiation, excited by square electrical pulses, with a fixed repetition rate of 10 MHz and varying electrical pulse durations $\Delta t_{ac} = 1.7$ and 5.0 ns, respectively. The experimental data (dots) are fitted by single-peak Gaussian fits (curves). (c) The light emission width $\Delta t_{ph}$ versus the corresponding electrical pulse width $\Delta t_{ac}$. Open circles are experimental data and dashed line is linear fit. (d) Light emission in response to ac voltage pulse injection at different repetition rates. The electrical pulse duration $\Delta t_{ac}$ was kept at 10 ns, while the repetition rates were selected as 40 MHz, 33.3 MHz, 20 MHz, and 10 MHz, respectively.

with near-perfect contrast. This unusual observation is attributed to the direct electron cooling of graphene into hBN, which is mediated by out-of-plane heat transfer enabled by electron–hyperbolic phonon coupling at the highly localized Gr/hBN interfaces, as demonstrated in recent theoretical and ultrafast photocurrent measurements [50–52].

### *2.4. Hot electrons cooling in graphene*

To further understand the microscopic mechanism, we investigated three main pathways of hot electrons cooling in graphene. The first is electron-optical phonon scattering. According to the theory and time-resolved spectroscopy studies, electrons with an energy that is high enough ($k_B T_e > 0.16\,eV$, $T_e > 1\,860\,K$) can efficiently emit optical phonons with scattering times $\tau_{op}$ well below 1 ps [53, 54]. Therefore, rapid thermalization occurs not only within the electronic system by electron–electron scattering, but also occurs between electrons and optical phonons due to electron-optical phonon scattering. The hot electrons are strongly coupled to the optical phonons of graphene and are in equilibrium, while optical phonons cool down to low-energy acoustic phonons much more slowly. The lifetime of optical phonon $\tau_{op-ap}$ in graphene has been measured by time-resolved Raman spectroscopy, yielding values in the order of a few ps [55]. Since hot optical phonons cannot cool down fast enough, they may heat the electron again. This hot phonon bottleneck causes electrons in graphene to have similar temperatures to optical phonons, while acoustic phonons have much lower temperatures. As shown in figures 3(b) and 5(a), in suspended graphene devices under high bias, the temperature of electrons is much higher than the temperature of lattice. That is, electrons are out-of-equilibrium with acoustic phonons in graphene and in hBN. The second cooling pathway is electron-acoustics phonon scattering. Electrons whose kinetic energy is not sufficient to couple with optical phonons can be coupled to acoustic

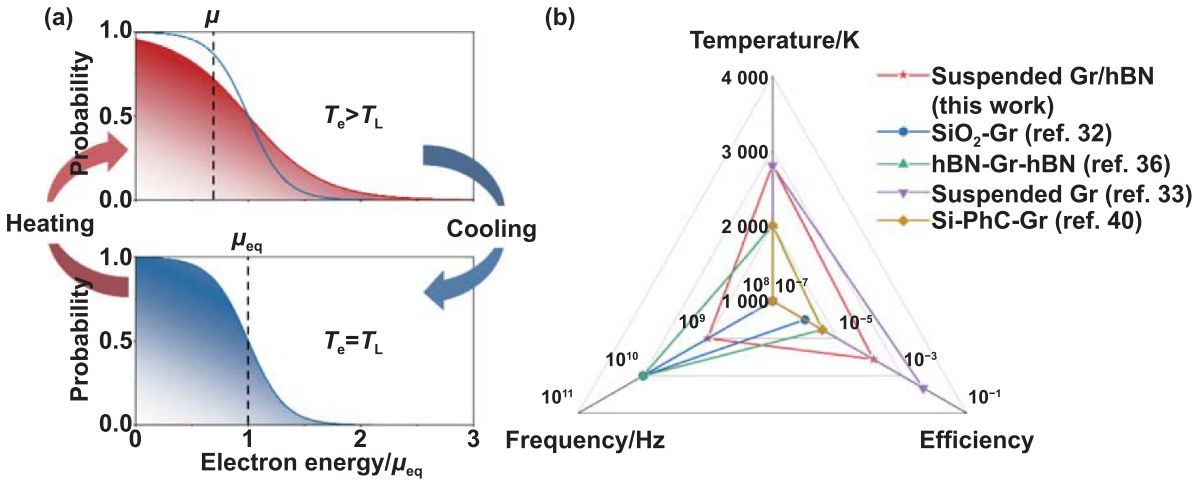


**Figure 5.** Mechanism and figure of merit of out-of-equilibrium light emission. (a) Schematic diagram of the heating and cooling of electrons in graphene, wherein in the hot state, the electron distribution is characterized by the carrier temperature $T_e$ greater than the lattice temperature $T_L$, and the 'hot' chemical potential $\mu$ less than the equilibrium chemical potential $\mu_{eq}$. (b) Comparison of the figures of merit of graphene emitters between this work and previous reports, including electronic temperature, modulation frequency and radiation efficiency.

phonons. Previous works have investigated the cooling of hot electrons in graphene by momentum-conservation scattering of acoustic phonons. The cooling channel typically results in a lifetime $\tau_{ap}$ on the order of ns, which is much less efficient than cooling through optical phonons [56, 57]. This is mainly due to the requirement of conservation of momentum and the large velocity mismatch between electrons and acoustic phonons. The last cooling channel is the substrate or interface phonons. Hot electrons in graphene can be relaxed by coupling to nearby substrate phonons (in our case, the bottom layers of hBN on top of graphene). Specifically, hBN is a natural hyperbolic material in which hyperbolic phonon polaritons occur in its two Reststrahlen bands. Since these two spectral regions have hyperbolic phonon polaritons, the hot electrons in Gr/hBN are cooled by out-of-plane coupling with hyperbolic phonon polaritons in hBN. Thus, the hot electrons in graphene can be cooled by near-field coupling to a large photonic density of states, resulting in ps cooling time of electrons [51, 52, 58, 59].

In our case, the excitation time of the electrical pulse is on the order of ns, which is much longer than the upper limit of ps optical phonon lifetime $\tau_{op}$. Thus, hot electrons in graphene are expected to strongly couple to and equilibrate with optical phonons of graphene. These phonons are connected to the acoustic phonon system by thermal conductance $\Gamma_1$ and then to the ambient temperature via $\Gamma_2$. The measured difference in the temperature of electrons and acoustic phonons, $T_e - T_{ap} = P/\Gamma_1$, provides an estimation of $\Gamma_1 \sim 32.5$ MW·m$^{-2}$·K$^{-1}$. This value is consistent with recent theoretical and experimental results [36, 60]. The measured cooling time $\tau_c \sim 0.9$ ns provides a measurement of the electron/phonon heat capacity of the system, $C = \tau_c\Gamma_1 = 2.9 \times 10^{-2}$ J·m$^{-2}$·K$^{-1}$, which is significantly larger than the electronic heat capacity alone, indicating the equilibrium of electrons and optical phonons. This value corresponds to optical phonons in graphene and a ~12 nm thick hBN layer on top of it [61]. This analysis is qualitatively consistent with the out -of-plane coupling of hot electrons in graphene to hyperbolic phonon polaritons in hBN. Observations of sub-ns cooling times in graphene support the assumption that hot electrons are efficiently cooled by coupling to hBN phonon polaritonic modes at the Gr/hBN interface rather than directly to acoustic phonons of graphene.

Based on the above analysis, the hBN capping layer on top of graphene not only provides strong adhesion to enhance the mechanical stability of the suspended devices, but also provides effective cooling pathways for hot electrons in graphene through out-of-plane coupling to hyperbolic phonon polaritons in hBN. Thus, the suspended Gr/hBN heterostructure light emitters demonstrated in this work simultaneously exhibits high stability and fast modulation speed of substrate-supported devices, as well as high electron temperature and high radiation efficiency of suspended devices. Furthermore, the monolithically sculpted vdW heterostructures offers the ability to design the spectrum through optical cavities, which can be further integrated into silicon photonic platform. Figure 5(b) summarizes the figures of merit of this work and previous reports, showing the best comprehensive performance of suspended Gr/hBN heterostructure thermal emitters.

## 3. Conclusions

In summary, here we established suspended Gr/hBN heterostructure devices as high-performance light emitters with high stability (~80% success rate of device fabrication), high radiation efficiency (~$1.3 \times 10^{-4}$, two orders of magnitude higher than graphene on substrates), and ultrafast electrical modulation rate (>1 GHz bandwidth). Elimination of substrate energy dissipation effectively generates hot electrons in biased suspended Gr/hBN devices, where the electrons acquire much higher temperature than the acoustic phonons and are not in

thermal equilibrium with the graphene lattices. By capping graphene with the top hBN layer, the interfacial vdW interaction not only provides strong adhesion to enhance the mechanical properties of suspended graphene, but also offers a rapid cooling pathway of hot electrons in graphene to the hyperbolic polariton modes in hBN, leading to ultrafast light emission from graphene. By integrated with silicon-based optical cavity, the emission spectrum of suspended Gr/hBN thermal emitters can be modified and enhanced in the near-infrared and the visible spectral range. The unique heat transfer mechanism, combined with the small volume and record-low heat capacity of graphene, makes it ideal for electrically driven ultrafast light sources, which are key components in high-performance photonic integrated circuits.

## 4. Methods

The thicknesses of graphene and hBN were measured by AFM (NT-MDT NTEGRA PRIMA). The Raman spectra of graphene and hBN were measured by a confocal micro-Raman spectrometer (Renishaw inVia Qontor), which uses a solid-state laser at 532 nm. The used grating is 1800 grooves $mm^{-1}$, and a spot size of the laser is about 500 nm. $I-V_b$ and $I-V_g$ characteristics were measured by a probe station (Lake Shore CRX-6.5 K Cryogenic Probe Station) with a source meter (Keithley 2636B). Thermal emission spectra were recorded using a spectrometer and an electrically cooled Si CCD with a 50× objective. The spectrometer is calibrated by quartz tungsten lamp at a temperature of 3200 K before measurement. All measurements are performed in a vacuum.

## Acknowledgments

This work is financially supported by the National Natural Science Foundation of China (Nos. 12174444 and 52202195), and the Natural Science Foundation of Hunan Province (2020RC3032).

## Author contributions

M Zhu conceived the idea, designed the experiment and wrote the manuscript. Q Liu fabricated the devices and carried out the measurements with the help of F Luo, X Li, T Zhang, and C Qin. W Xu and Z Zhu carried out the calculations of heat transfer and emission spectrum. S Qin and K S Novoselov supervised this project. All authors have given approval to the manuscript.

## Conflict of interest

The authors declare no conflicting interest.

## ORCID iD

Mengjian Zhu https://orcid.org/0000-0002-7863-2660

## References

[1] Shalf J 2020 The future of computing beyond Moore's law *Phil. Trans. R. Soc.* A **378** 20190061
[2] Heck M J, Bauters J F, Davenport M L, Doylend J K, Jain S, Kurczveil G, Srinivasan S, Tang Y B and Bowers J E 2013 Hybrid silicon photonic integrated circuit technology *IEEE J. Sel. Top. Quantum Electron.* **19** 6100117
[3] Bogaerts W, Pérez D, Capmany J, Miller D A B, Poon J, Englund D, Morichetti F and Melloni A 2020 Programmable photonic circuits *Nature* **586** 207–16
[4] Bonaccorso F, Sun Z, Hasan T and Ferrari A C 2010 Graphene photonics and optoelectronics *Nat. Photon.* **4** 611–22
[5] Romagnoli M, Sorianello V, Midrio M, Koppens F H L, Huyghebaert C, Neumaier D, Galli P, Templ W, D'errico A and Ferrari A C 2018 Graphene-based integrated photonics for next-generation datacom and telecom *Nat. Rev. Mater.* **3** 392–414
[6] Akinwande D, Huyghebaert C, Wang C H, Serna M I, Goossens S, Li L J, Wong H S P and Koppens F H L 2019 Graphene and two-dimensional materials for silicon technology *Nature* **573** 507–18
[7] Koppens F H L, Mueller T, Avouris P, Ferrari A C, Vitiello M S and Polini M 2014 Photodetectors based on graphene, other two-dimensional materials and hybrid systems *Nat. Nanotechnol.* **9** 780–93
[8] Xia F N, Mueller T, Lin Y M, Valdes-Garcia A and Avouris P 2009 Ultrafast graphene photodetector *Nat. Nanotechnol.* **4** 839–43
[9] Gan X T, Shiue R J, Gao Y D, Meric I, Heinz T F, Shepard K, Hone J, Assefa S and Englund D 2013 Chip-integrated ultrafast graphene photodetector with high responsivity *Nat. Photon.* **7** 883–7
[10] Mueller T, Xia F N and Avouris P 2010 Graphene photodetectors for high-speed optical communications *Nat. Photon.* **4** 297–301
[11] Pospischil A, Humer M, Furchi M M, Bachmann D, Guider R, Fromherz T and Mueller T 2013 CMOS-compatible graphene photodetector covering all optical communication bands *Nat. Photon.* **7** 892–6
[12] Yoshioka K, Wakamura T, Hashisaka M, Watanabe K, Taniguchi T and Kumada N 2022 Ultrafast intrinsic optical-to-electrical conversion dynamics in a graphene photodetector *Nat. Photon.* **16** 718–23
[13] Koepfli S M *et al* 2023 Metamaterial graphene photodetector with bandwidth exceeding 500 gigahertz *Science* **380** 1169–74
[14] Liu M, Yin X B, Ulin-Avila E, Geng B S, Zentgraf T, Ju L, Wang F and Zhang X 2011 A graphene-based broadband optical modulator *Nature* **474** 64–67
[15] Liu M, Yin X B and Zhang X 2012 Double-layer graphene optical modulator *Nano Lett.* **12** 1482–5
[16] Phare C T, Daniel Lee Y H, Cardenas J and Lipson M 2015 Graphene electro-optic modulator with 30 GHz bandwidth *Nat. Photon.* **9** 511–4
[17] Agarwal H *et al* 2021 2D-3D integration of hexagonal boron nitride and a high-κ dielectric for ultrafast graphene-based electro-absorption modulators *Nat. Commun.* **12** 1070
[18] Heidari E, Dalir H, Koushyar F M, Nouri B M, Patil C, Miscuglio M, Akinwande D and Sorger V J 2022 Integrated ultra-high-performance graphene optical modulator *Nanophotonics* **11** 4011–6
[19] Dalir H, Xia Y, Wang Y and Zhang X 2016 Athermal broadband graphene optical modulator with 35 GHz speed *ACS Photonics* **3** 1564–8
[20] Sorianello V, Midrio M, Contestabile G, Asselberghs I, van Campenhout J, Huyghebaert C, Goykhman I, Ott A K, Ferrari A C and Romagnoli M 2018 Graphene–silicon

phase modulators with gigahertz bandwidth *Nat. Photon.* **12** 40–44
[21] Youngblood N, Anugrah Y, Ma R, Koester S J and Li M 2014 Multifunctional graphene optical modulator and photodetector integrated on silicon waveguides *Nano Lett.* **14** 2741–6
[22] Lui C H, Mak K F, Shan J and Heinz T F 2010 Ultrafast photoluminescence from graphene *Phys. Rev. Lett.* **105** 127404
[23] Huang D *et al* 2018 Gate switching of ultrafast photoluminescence in graphene *Nano Lett.* **18** 7985–90
[24] Mak K F, Ju L, Wang F and Heinz T F 2012 Optical spectroscopy of graphene: from the far infrared to the ultraviolet *Solid State Commun.* **152** 1341–9
[25] Paul K K, Kim J H and Lee Y H 2021 Hot carrier photovoltaics in van der Waals heterostructures *Nat. Rev. Phys.* **3** 178–92
[26] Rezaeifar F, Ahsan R, Lin Q F, Chae H U and Kapadia R 2019 Hot-electron emission processes in waveguide-integrated graphene *Nat. Photon.* **13** 843–8
[27] Kim L, Kim S, Jha P K, Brar V W and Atwater H A 2021 Mid-infrared radiative emission from bright hot plasmons in graphene *Nat. Mater.* **20** 805–11
[28] Freitag M, Chiu H Y, Steiner M, Perebeinos V and Avouris P 2010 Thermal infrared emission from biased graphene *Nat. Nanotechnol.* **5** 497–501
[29] Berciaud S, Han M Y, Mak K F, Brus L E, Kim P and Heinz T F 2010 Electron and optical phonon temperatures in electrically biased graphene *Phys. Rev. Lett.* **104** 227401
[30] Chae D H, Krauss B, von Klitzing K and Smet J H 2010 Hot phonons in an electrically biased graphene constriction *Nano Lett.* **10** 466–71
[31] Luxmoore I J, Adlem C, Poole T, Lawton L M, Mahlmeister N H and Nash G R 2013 Thermal emission from large area chemical vapor deposited graphene devices *Appl. Phys. Lett.* **103** 131906
[32] Miyoshi Y, Fukazawa Y, Amasaka Y, Reckmann R, Yokoi T, Ishida K, Kawahara K, Ago H and Maki H 2018 High-speed and on-chip graphene blackbody emitters for optical communications by remote heat transfer *Nat. Commun.* **9** 1279
[33] Kim Y D *et al* 2015 Bright visible light emission from graphene *Nat. Nanotechnol.* **10** 676–81
[34] Dorgan V E, Behnam A, Conley H J, Bolotin K I and Pop E 2013 High-field electrical and thermal transport in suspended graphene *Nano Lett.* **13** 4581–6
[35] Chen C Y, Rosenblatt S, Bolotin K I, Kalb W, Kim P, Kymissis I, Stormer H L, Heinz T F and Hone J 2009 Performance of monolayer graphene nanomechanical resonators with electrical readout *Nat. Nanotechnol.* **4** 861–7
[36] Kim Y D *et al* 2018 Ultrafast graphene light emitters *Nano Lett.* **18** 934–40
[37] Barnard H R, Zossimova E, Mahlmeister N H, Lawton L M, Luxmoore I J and Nash G R 2016 Boron nitride encapsulated graphene infrared emitters *Appl. Phys. Lett.* **108** 131110
[38] Son S K *et al* 2017 Graphene hot-electron light bulb: incandescence from hBN-encapsulated graphene in air *2D Mater.* **5** 011006
[39] Luo F *et al* 2019 Graphene thermal emitter with enhanced joule heating and localized light emission in air *ACS Photonics* **6** 2117–25
[40] Shiue R J, Gao Y D, Tan C, Peng C, Zheng J B, Efetov D K, Kim Y D, Hone J and Englund D 2019 Thermal radiation control from hot graphene electrons coupled to a photonic crystal nanocavity *Nat. Commun.* **10** 109
[41] Zhang T Y *et al* 2022 A monolithically sculpted van der Waals nano-opto-electro-mechanical coupler *Light Sci. Appl.* **11** 48
[42] Wang L *et al* 2013 One-dimensional electrical contact to a two-dimensional material *Science* **342** 614–7
[43] Falin A *et al* 2017 Mechanical properties of atomically thin boron nitride and the role of interlayer interactions *Nat. Commun.* **8** 15815
[44] Dean C R *et al* 2010 Boron nitride substrates for high-quality graphene electronics *Nat. Nanotechnol.* **5** 722–6
[45] Fong K C, Wollman E E, Ravi H, Chen W, Clerk A A, Shaw M D, Leduc H G and Schwab K C 2013 Measurement of the electronic thermal conductance channels and heat capacity of graphene at low temperature *Phys. Rev.* X **3** 041008
[46] Kokkoniemi R *et al* 2020 Bolometer operating at the threshold for circuit quantum electrodynamics *Nature* **586** 47–51
[47] Massicotte M, Soavi G, Principi A and Tielrooij K J 2021 Hot carriers in graphene—fundamentals and applications *Nanoscale* **13** 8376–411
[48] Ferrari A C and Basko D M 2013 Raman spectroscopy as a versatile tool for studying the properties of graphene *Nat. Nanotechnol.* **8** 235–46
[49] Pop E, Varshney V and Roy A K 2012 Thermal properties of graphene: fundamentals and applications *MRS Bull.* **37** 1273–81
[50] Kumar A, Low T, Fung K H, Avouris P and Fang N X 2015 Tunable light-matter interaction and the role of hyperbolicity in graphene-hBN system *Nano Lett.* **15** 3172–80
[51] Tielrooij K J *et al* 2018 Out-of-plane heat transfer in van der Waals stacks through electron-hyperbolic phonon coupling *Nat. Nanotechnol.* **13** 41–46
[52] Principi A, Lundeberg M B, Hesp N C H, Tielrooij K J, Koppens F H L and Polini M 2017 Super-planckian electron cooling in a van der Waals stack *Phys. Rev. Lett.* **118** 126804
[53] Piscanec S, Lazzeri M, Mauri F, Ferrari A C and Robertson J 2004 Kohn anomalies and electron-phonon interactions in graphite *Phys. Rev. Lett.* **93** 185503
[54] Sohier T, Calandra M, Park C H, Bonini N, Marzari N and Mauri F 2014 Phonon-limited resistivity of graphene by first-principles calculations: electron-phonon interactions, strain-induced gauge field, and Boltzmann equation *Phys. Rev.* B **90** 125414
[55] Wu S W, Liu W T, Liang X G, Schuck P J, Wang F, Shen Y R and Salmeron M 2012 Hot phonon dynamics in graphene *Nano Lett.* **12** 5495–9
[56] Kaasbjerg K, Thygesen K S and Jacobsen K W 2012 Unraveling the acoustic electron-phonon interaction in graphene *Phys. Rev.* B **85** 165440
[57] Bistritzer R and MacDonald A H 2009 Electronic cooling in graphene *Phys. Rev. Lett.* **102** 206410
[58] Yang W *et al* 2018 A graphene Zener-Klein transistor cooled by a hyperbolic substrate *Nat. Nanotechnol.* **13** 47–52
[59] Caldwell J D *et al* 2014 Sub-diffractional volume-confined polaritons in the natural hyperbolic material hexagonal boron nitride *Nat. Commun.* **5** 5221
[60] Low T, Perebeinos V, Kim R, Freitag M and Avouris P 2012 Cooling of photoexcited carriers in graphene by internal and substrate phonons *Phys. Rev.* B **86** 045413
[61] Cocemasov A I, Nika D L and Balandin A A 2015 Engineering of the thermodynamic properties of bilayer graphene by atomic plane rotations: the role of the out-of-plane phonons *Nanoscale* **7** 12851–9